

Cite this: *Chem. Sci.*, 2011, **2**, 1782

www.rsc.org/chemicalscience

EDGE ARTICLE

# Chemical control of interstitial iron leading to superconductivity in $\text{Fe}_{1+x}\text{Te}_{0.7}\text{Se}_{0.3}$ <sup>†</sup>

Efrain E. Rodriguez,<sup>a</sup> Christopher Stock,<sup>ab</sup> Ping-Yen Hsieh,<sup>ac</sup> Nicholas P. Butch,<sup>d</sup> Johnpierre Paglione<sup>d</sup> and Mark A. Green<sup>\*ac</sup>

Received 26th February 2011, Accepted 16th June 2011

DOI: 10.1039/c1sc00114k

Although it possesses the simple layered topology of the tetragonal anti-PO structure, the Fe(Te,Se) series has a complex structural and magnetic phase diagram that is dependent on composition and occupancy of a secondary interstitial Fe site. Here we show that superconductivity in  $\text{Fe}_{1+x}\text{Te}_{0.7}\text{Se}_{0.3}$  is enhanced by topotactic deintercalation of the interstitial iron with iodine, demonstrating the competing roles of the two iron positions. We follow the evolution of the structure and magnetic properties as a function of interstitial iron. Powder neutron diffraction reveals a flattening of the  $\text{Fe}(\text{Te},\text{Se})_4$  tetrahedron on Fe removal and an unusual temperature dependence of the lattice parameters that increases strongly below 150 K along with lattice strain. Inelastic neutron scattering shows gapless paramagnetic scattering evolves into a gapped excitation at 6 meV on removal of interstitial iron. This work highlights the robustness of the superconductivity across different Fe(Te,Se) compositions and geometries.

## Introduction

Iron based high temperature superconductors offer new opportunities to establish the interplay between magnetism, composition and electronic properties.<sup>1</sup> Several structural families have now been established since the discovery of superconductivity at 26 K in  $\text{LaO}_{1-x}\text{F}_x\text{FeAs}$ .<sup>2</sup> These iron pnictide systems require additional cations to provide charge balancing, which is not necessary in the structurally simpler superconducting iron chalcogenide series,  $\text{FeX}$  (X = Te, Se, S).<sup>3-5</sup> Within this series, stoichiometric FeSe is orthorhombic and superconducting at 8.5 K,<sup>3,6</sup> which increases to 36.7 K under high pressure.<sup>7-9</sup> The work on stoichiometric FeSe,<sup>6</sup> as with studies on  $\text{Li}_{1-y}\text{Fe}_{1+y}\text{As}$ ,<sup>10</sup> demonstrates the very rapid suppression of superconductivity with composition.  $\text{Fe}_{1+x}\text{Te}$  can only be synthesized with large

amounts of interstitial iron. This additional iron is known to greatly affect its structural and magnetic properties. For example, for  $x > 0.12$  the tetragonal structure transforms to a orthorhombic one with an incommensurate magnetic structure at low temperature, in contrast to the monoclinic symmetry and a commensurate magnetic structure for lower iron levels.<sup>11</sup> Using conventional solid state chemistry methodology, it was reported that  $\text{Fe}_{1+x}\text{Te}$  can be formed at least over a range from  $\text{Fe}_{1.076(2)}\text{Te}$  to  $\text{Fe}_{1.141(2)}\text{Te}$ .<sup>11</sup> Additional control of the concentration can be achieved by deintercalation of the interstitial iron with iodine, transforming  $\text{Fe}_{1.18(5)}\text{Te}$  to  $\text{Fe}_{1.042(5)}\text{Te}$ .<sup>12</sup>

Previous studies on  $\text{Fe}_{1+x}\text{Te}_{1-y}\text{Se}_y$  have noted that optimal superconductivity has been limited to compositions around  $y \sim 0.5$ .<sup>13</sup> However, a strong correlation has also been reported between anion composition and the amount of interstitial iron present for both the Fe(Te,Se)<sup>13</sup> and Fe(Te,S)<sup>14</sup> phase diagrams. The Se or S substitution reduces the lattice volume, imposes chemical pressure, and suppresses the amount of interstitial iron present. It is therefore unclear whether the particular compositions that are noted for their superconductivity are a result of optimal Te : Se ratios or whether the presence of interstitial iron, despite occupancies of only a few percent, is playing the prevailing role on the electronic properties. Previous attempts to study the effect of interstitial iron on the structural and magnetic properties of the  $\text{Fe}_{1+x}(\text{Te},\text{Se})$  series have shown that interstitial iron may be detrimental to the superconductivity.<sup>15-17</sup> However, the interstitial iron content is coupled with the Te : Se ratio, and all previous attempts to synthesize samples with different iron content also result in variation of the Te : Se ratio, as evidenced

<sup>a</sup>NIST Center for Neutron Research, NIST, Gaithersburg, MD, 20899, USA. E-mail: mark.green@nist.gov

<sup>b</sup>Indiana University, 2401 Milo B. Sampson Lane, Bloomington, Indiana, 47408, USA

<sup>c</sup>Department of Materials Science and Engineering, University of Maryland, College Park, 20742, USA

<sup>d</sup>Center for Nanophysics and Advanced Materials, University of Maryland, College Park, MD, 20742, USA

<sup>†</sup> Electronic supplementary information (ESI) available: S1-3 contains typical diffraction patterns obtained using the Ge311 and Cu311 monochromator along with more information of the isotropic Gaussian strain. S4 is a contour plot of the temperature variation of the (200) and (111) reflections. Table S1 contains The structural parameters as a function of temperature including goodness-of-fit factors. See DOI: 10.1039/c1sc00114k

by variation of lattice parameters.<sup>16,17</sup> Here, we take a single batch of  $\text{Fe}_{1.048(2)}\text{Te}_{0.7}\text{Se}_{0.3}$  and topotactically deintercalate different amounts of excess iron with iodine, producing a range of compositions at a fixed Te : Se ratio, where the lattice parameter,  $c$ , varies by only 0.0037(2) Å across all compositions. We show that the secondary interstitial iron is the critical parameter and superconductivity in other Te : Se ratios can be artificially produced by removal of the interstitial iron. The  $\text{Fe}_{1+x}\text{Te}_{0.7}\text{Se}_{0.3}$  composition with 70 : 30 ratio of Te : Se was specifically chosen as it has been previously reported as having both a very high<sup>18</sup> and very low<sup>13,19</sup> superconducting volume fraction.

## Results and discussion

A powder sample of nominal composition,  $\text{Fe}_{1.05}\text{Te}_{0.7}\text{Se}_{0.3}$ , was synthesized by a solid state reaction of the constituent elements at 700 °C under vacuum. The energy dispersive X-ray (EDX) technique was found not to be sufficiently accurate to determine the occupancy of the iron interstitial sites. It has been reported that the occupancy values obtained for bulk single crystal X-ray diffraction determination and EDX measurements, which is a surface probe, yield different values.<sup>13</sup> This implies that the stability of the excess iron is less on the surface and the iron adopts more locations in the bulk of the sample. Single crystal X-ray diffraction and powder neutron diffraction were found to give consistent and reliable values for the average composition. Samples of  $\text{Fe}_{1+x}\text{Te}_{0.7}\text{Se}_{0.3}$  were, therefore, characterized by high-resolution powder neutron diffraction using the BT1 diffractometer at NIST. For composition analysis, the samples were cooled to 100 K to reduce the thermal factors that can correlate with the occupancy values, and measured using the Cu 311 monochromator at the high 90° take-off angle, giving  $\lambda = 1.5401$  Å. Temperature dependence of the lattice parameters and isotropic strain were performed using the Ge 311 monochromator at a 75° take-off angle, giving a wavelength,  $\lambda = 2.0787$  Å. The actual composition was determined to be  $\text{Fe}_{1.048(2)}\text{Te}_{0.7}\text{Se}_{0.3}$ .

The composition  $\text{Fe}_{1.048(2)}\text{Te}_{0.7}\text{Se}_{0.3}$  was then divided into 4 batches, three of which were exposed to different levels of  $\text{I}_2$  vapour at 200 °C in an evacuated glass ampoule, which topotactically deintercalates the excess iron.<sup>12</sup> The samples were subsequently washed with methanol to remove the  $\text{FeI}_2$  formed in the reaction, sonicated and centrifuged. A small (<1%) impurity of  $\text{FeTe}_2$  were present in samples that have been reacted with  $\text{I}_2$ . Powder neutron diffraction at  $\lambda = 1.5401$  Å determined the compositions of these to be  $\text{Fe}_{1.033(2)}\text{Te}_{0.7}\text{Se}_{0.3}$ ,  $\text{Fe}_{1.018(2)}\text{Te}_{0.7}\text{Se}_{0.3}$  and  $\text{Fe}_{1.009(3)}\text{Te}_{0.7}\text{Se}_{0.3}$ . All refinements, which were carried out with the FULLPROF suite,<sup>20</sup> gave the ratio of Te : Se to be 70 : 30 within the accuracy of the experiments, therefore this parameter was not included further in the refinements. A summary of the structural parameters for all four compositions at 100 K is given in Table 1.

The  $c$  lattice parameter varies smoothly with Se incorporation into  $\text{Fe}_{1+x}\text{Te}^4$ , and which therefore offers a secondary approach to evaluate the composition. In our samples, the  $c$  parameter under ambient conditions refined to be 6.1165(1) Å, 6.11974(7) Å, 6.12021(7) Å and 6.12021(12) Å for  $\text{Fe}_{1.048(2)}\text{Te}_{0.7}\text{Se}_{0.3}$ ,  $\text{Fe}_{1.033(2)}\text{Te}_{0.7}\text{Se}_{0.3}$ ,  $\text{Fe}_{1.018(2)}\text{Te}_{0.7}\text{Se}_{0.3}$  and  $\text{Fe}_{1.009(3)}\text{Te}_{0.7}\text{Se}_{0.3}$ , respectively. This represents a maximum change of  $c = 0.0037(2)$

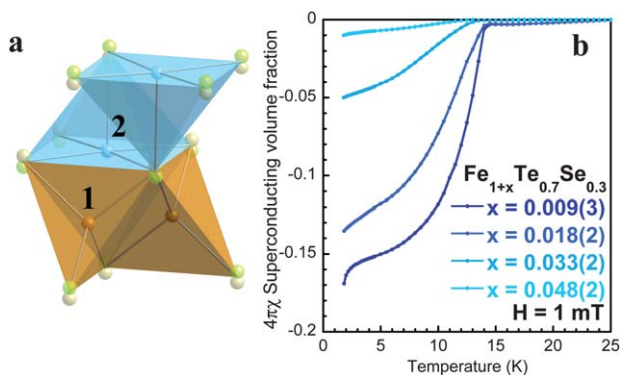
between all phases, confirming that the interstitial iron has a very minor effect on the lattice parameter, which are almost wholly controlled by the composition. Producing different iron concentrations by low temperature deintercalation of a single  $\text{Fe}_{1+x}\text{Te}_{1-y}\text{Se}_y$  batch, eliminates Te : Se composition variation effects, which are evident in experiments that attempt to synthesize different compositions by direct reaction of elements with varying nominal composition. For example, the iodine deintercalation samples have a variation of the  $c$  lattice parameters that is 5 times less than those obtained using direct reactions.<sup>16,17</sup> In addition, studies have also demonstrated that experimentally determined excess iron composition can be identical irrespective of the nominal composition used.<sup>17</sup> This iodine deintercalation technique therefore allows for accurate experiments to be performed on the variation of Fe content at a fixed Te : Se ratio.

Fig. 1, panel a, shows the two iron locations in the anti-PbO structure of  $\text{Fe}_{1+x}\text{Te}_{0.7}\text{Se}_{0.3}$ . The fully occupied iron, shaded orange, forms the main  $\text{Fe}(\text{Te},\text{Se})_4$  tetrahedron that is edge shared to form two dimensional layers. The nearest neighbour van der Waals bonded layers are shifted by  $(\frac{1}{2} \frac{1}{2})$  in the  $ab$  plane. The partially occupied Fe sites, which in the case of  $\text{Fe}_{1+x}\text{Fe}_{0.7}\text{Se}_{0.3}$  can adopt occupancies of up to ~5%, sits directly above, and bonded to, the (Te, Se) split site in the layer below. It is further bonded to four other (Te, Se) sites within the  $ab$  plane to form a square pyramidal arrangement. Magnetization measurements, using a commercial SQUID magnetometer, were performed under zero-field cooled conditions on the four variable iron concentrations,  $\text{Fe}_{1.048(2)}\text{Te}_{0.7}\text{Se}_{0.3}$ ,  $\text{Fe}_{1.033(2)}\text{Te}_{0.7}\text{Se}_{0.3}$ ,  $\text{Fe}_{1.018(2)}\text{Te}_{0.7}\text{Se}_{0.3}$  and  $\text{Fe}_{1.009(3)}\text{Te}_{0.7}\text{Se}_{0.3}$  and are shown in Fig. 1, panel b.  $\text{Fe}_{1.048(2)}\text{Te}_{0.7}\text{Se}_{0.3}$  showed extremely low superconducting volume fractions. The extent of the superconducting volume fraction steadily increases with the removal of the interstitial iron, establishing a direct association between the two. The iodine deintercalation procedure is a topotactic technique that is done at very low temperatures, which are much below the synthesis temperature, thereby ruling out any possible changes to the actual  $\text{Fe}_{1+x}\text{Te}_{0.7}\text{Se}_{0.3}$  framework. In addition, the superconducting transition temperature is found to increase from 13.3 K to 14.5 K as a function of interstitial iron content (see Table 1). The value of 14.5 K is similar to the highest value for the superconducting transition temperature found in the  $\text{Fe}(\text{Te},\text{Se})$  series, and suggests a common origin for superconductivity across the series.

Fig. 2, panel a and b, shows the lattice parameter as a function of temperature for the four compositions, as obtained from Rietveld refinements of powder neutron diffraction data. Each of the materials undergo unusual expansion of the  $ab$  plane below ~125 K, whilst the  $c$  parameter shrinks in a typical linear fashion. Similar anisotropic thermal expansion has been previously reported in other members of the  $\text{Fe}_{1+x}(\text{Te},\text{Se})$  series.<sup>21–23</sup> The isotropic strain of the system, shown in Fig. 2 panel c, obtained from the peak shape parameters of the refinements, increases greatly below 150 K. The increase in both the lattice parameter and strain below 150 K suggests that the expansion in  $ab$ , which is directly related to the primary Fe–Fe distance, is a result of microstrain within the lattice. Analysis of the peak broadening (see supplementary information) ruled out the strain to be a result of a small orthorhombic distortion or even orthorhombic strain on a tetragonal lattice. Therefore the

**Table 1** Crystallographic parameters for four compositions of general formula,  $\text{Fe}_{1+x}\text{Te}_{0.7}\text{Se}_{0.3}$ , obtained by Rietveld refinements of powder neutron diffraction data at 7 and 100 K. The structure was solved in the  $P4/nmm$  space group, with the main layered framework at Fe (0.75 0.25 0.5), Se and Te at offset at (0.25 0.25  $z$ ) and the interstitial Fe2 metal at (0.25 0.25  $z$ )

	$\text{Fe}_{1.009(3)}\text{Fe}_{0.7}\text{Se}_{0.3}$ 100 K	$\text{Fe}_{1.018(2)}\text{Fe}_{0.7}\text{Se}_{0.3}$ 100 K	$\text{Fe}_{1.033(2)}\text{Fe}_{0.7}\text{Se}_{0.3}$ 100 K	$\text{Fe}_{1.048(2)}\text{Fe}_{0.7}\text{Se}_{0.3}$ 100 K
$\text{Te}_z$	0.2136(7)	0.2127(5)	0.2109(4)	0.2101(3)
$\text{Se}_z$	0.262(1)	0.2607(9)	0.2600(7)	0.2614(6)
$\text{Fe}2_z$	0.72(2)	0.72(1)	0.749(5)	0.774(3)
Fe2 occ	0.009(3)	0.018(2)	0.033(2)	0.048(2)
$a/\text{\AA}$	3.80197(4)	3.80166(2)	3.79971(2)	3.79984(2)
$c/\text{\AA}$	6.08062(9)	6.07568(6)	6.07990(5)	6.08386(4)
$V/\text{\AA}^3$	87.895(2)	87.809(1)	87.780(1)	87.843(1)
$R_p$	4.85	5.05	5.00	4.12
$wR_p$	6.99	6.54	6.83	5.72
$\chi^2$	2.04	1.38	1.76	1.77
	$\text{Fe}_{1.009(3)}\text{Fe}_{0.7}\text{Se}_{0.3}$ 7 K	$\text{Fe}_{1.018(2)}\text{Fe}_{0.7}\text{Se}_{0.3}$ 7 K	$\text{Fe}_{1.033(2)}\text{Fe}_{0.7}\text{Se}_{0.3}$ 7 K	$\text{Fe}_{1.048(2)}\text{Fe}_{0.7}\text{Se}_{0.3}$ 7 K
$\text{Te}_z$	0.2155(7)	0.2126(4)	0.2106(4)	0.2107(3)
$\text{Se}_z$	0.262(1)	0.2615(7)	0.2609(7)	0.2611(5)
$\text{Fe}2_z$	0.72(2)	0.709(8)	0.763(5)	0.776(2)
Fe2 occ	0.009(—)	0.018(—)	0.033(—)	0.048(—)
$a/\text{\AA}$	3.80429(4)	3.80184(2)	3.80023(2)	3.80136(2)
$c/\text{\AA}$	6.06688(9)	6.07415(5)	6.07704(5)	6.07420(4)
$V/\text{\AA}^3$	87.804(2)	87.796(1)	87.763(1)	87.774(1)
$R_p$	4.73	4.19	5.07	3.70
$wR_p$	6.85	5.55	6.90	5.32
$\chi^2$	1.91	1.60	1.78	1.82
$T_c/\text{K}$	14.5	14.3	13.8	13.3



**Fig. 1** Panel a: Structure of  $\text{Fe}_{1+x}\text{Te}_{0.7}\text{Se}_{0.3}$ , highlighting the two distinct iron locations; 1 forms the edge shared tetrahedral layers, while the partially occupied (< 5%) square pyramidal site 2 lies within the (Te, Se) plane. The Te and Se adopt very different positions along the  $z$  axis, creating a split site anion distribution. Panel b: Interstitial iron in  $\text{Fe}_{1+x}\text{Te}_{0.7}\text{Se}_{0.3}$  is the dominant factor controlling the balance between superconductivity and localized magnetism, as measure by a commercial SQUID magnetometer.

strain results from structural effects accumulating from the stacking of the layers and the disorder caused by the mixed Te and Se sites that have very different Fe–Te and Fe–Se bond distances. It is interesting to note that there is an overall increase in the  $ab$  plane on reduction of the interstitial iron, reflecting the attractive bonding involving the interstitial iron within the van der Waals layers. The distance between the layers is almost identical for all compositions. A graphical comparison of the effect of iron deintercalation on the structure is given in Fig. 3 panel a.

As a comparison with  $\text{Fe}_{1.009(3)}\text{Te}_{0.7}\text{Se}_{0.3}$ , we determined by powder neutron diffraction, the structure of  $\text{Fe}_{1.008(3)}\text{Te}_{0.48(1)}\text{Se}_{0.52(2)}$  and find some stark contrasts between their structures. The former has lattice parameters of  $a = 3.80429(4)$  Å and  $c = 6.06688(9)$  Å at 5 K, whereas the latter possesses lattice parameters of  $a = 3.79496(5)$  Å and  $c = 5.91966(12)$  Å at 5 K. The Fe–Fe distance is directly related to the lattice parameter, such that  $d_{\text{Fe-Fe}} = a/\sqrt{2}$ . Therefore, the small change in  $a$  of  $\sim 0.01$  Å, suggests that the Fe–Fe distances within the  $ab$  plane are relatively insensitive to the anion composition. Similarly, the Fe–Te and Fe–Se bond lengths and angles are relatively unchanged between for the two compositions, and remain almost identical to the values found for their parent  $\text{Fe}_{1+x}\text{Te}$  and  $\text{FeSe}$  structures. In contrast, significant differences in bond distances along the  $c$  direction are observed; the 70 : 30 composition has significant shrinkage in the Fe tetrahedron or intralayers, but an increase between the van der Waals gap or interlayer spacing of  $\sim 0.24$  Å, which results in an overall increase in  $c$  of  $\sim 0.15$  Å, when compared with the 50 : 50 composition. As the superconducting transition temperatures are very similar in both compositions at  $\sim 14.5$  K, this confirms that the layer distances, and parameters related to this distance such as anion height, are not critical parameters in controlling the superconductivity. A detailed comparison of the two Fe environments is given in Fig. 3, panel b.

To understand the effects of deintercalation on the magnetic fluctuations in  $\text{Fe}_{1+x}(\text{Te,Se})$ , we performed inelastic neutron scattering measurements; the results are summarised in Fig. 4. The sample with the lowest concentration of excess iron and largest superconducting volume fraction shows a distinct feature centred at a  $|\mathbf{Q}| \approx 1.4$  Å<sup>-1</sup> and with an energy gap between 6 and 8 meV. This excitation has previously been observed below the

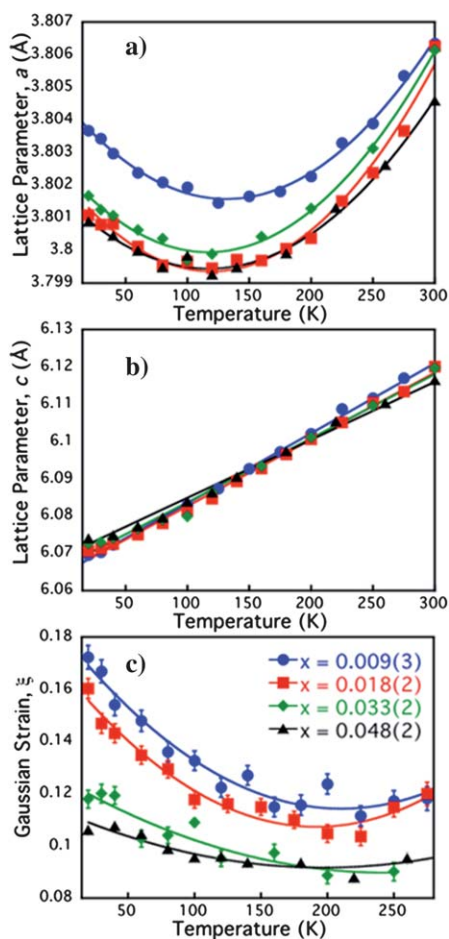


**Fig. 2** Panel a: Deintercalation of iron expands the  $ab$  lattice parameters which all also show an initial decrease on cooling from ambient conditions to 100 K, followed by an expansion to base whereas, Panel b: the  $c$  parameter is not greatly influenced by composition and shows a typical linear contraction with temperature. Panel c: Isotropic Gaussian strain within the lattice increases on both deintercalation of interstitial iron and on cooling. Error bars are shown for all figures and represent one standard deviation.

superconducting transition temperature in the compositions close to  $\text{FeTe}_{0.5}\text{Se}_{0.5}$  and is thought to be associated with the superconducting state.<sup>1,19,24,25</sup> As the interstitial iron concentration is increased, paramagnetic fluctuations fill in the energy gap, starting from  $|\mathbf{Q}| \approx 0.9 \text{ \AA}^{-1}$  close to the elastic line and dispersing towards the position of the gapped excitation (Fig. 4). For the sample with the maximum amount of excess iron,  $\text{Fe}_{1.048(2)}\text{Te}_{0.7}\text{Se}_{0.3}$ , this paramagnetic scattering completely overwhelms any gapped excitation that may have been present. The inelastic spectra clearly indicate that small changes in the interstitial iron concentration, even by a few percent, are critical to the electronic and magnetic properties of the  $\text{Fe}_{1+x}(\text{Te},\text{Se})$  superconductors.

There is substantial evidence pointing towards a direct coupling between antiferromagnetism and superconductivity in iron based superconductors. Mostly notably, strong magnetic collective excitations have been observed in both  $\text{Ba}_{0.6}\text{K}_{0.4}\text{Fe}_2\text{As}_2$ <sup>26</sup> and  $\text{Fe}(\text{Te},\text{Se})$ <sup>19,24,25</sup> systems and have been thought to directly result from the presence of an electronic superconducting energy

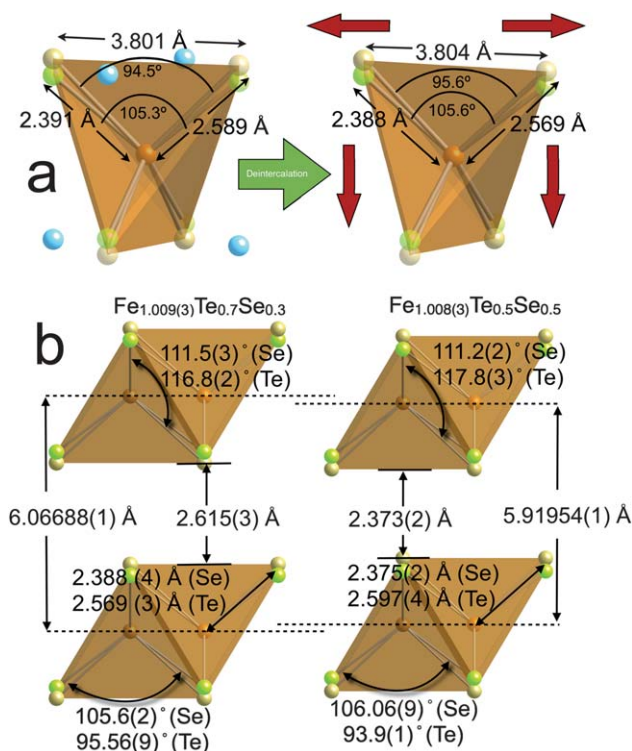


**Fig. 3** Panel a: Comparison of the structures at 7 K of  $\text{Fe}_{1+x}\text{Te}_{0.7}\text{Se}_{0.3}$  before and after removal of the interstitial iron with iodine, showing the deintercalation process increases the Fe–Fe distances while squashing the Fe tetrahedron in the  $c$  direction. Panel b: Comparison of the structures of  $\text{Fe}_{1.009(3)}\text{Te}_{0.7}\text{Se}_{0.3}$  with  $\text{Fe}_{1.008(3)}\text{Te}_{0.5}\text{Se}_{0.5}$ . The greatly increased  $c$  parameter in the 70 : 30 over the 50 : 50 composition of around 0.15 Å, combined with the collapse of the  $\text{Fe}(\text{Te}_{0.7}\text{Se}_{0.3})$  tetrahedron demonstrated in the less acute Te–Fe–Te bond angles and shorter Fe–Te bond distances, results in a significantly increased interlayer separation of  $\sim 0.24 \text{ \AA}$ . The superconducting  $T_c$  is unaffected by these structural changes.

gap. The collective mode has been found to be gapped and to draw spectral weight from lower energies in these systems, conserving sum rules required in neutron scattering. Furthermore, inelastic neutron studies of other superconductors where magnetism is thought to play an important role, such as  $\text{CeCu}_2\text{Si}_2$ ,<sup>27</sup>  $\text{CeCoIn}_5$ ,<sup>28</sup> and  $\text{YBa}_2\text{Cu}_3\text{O}_{6.5}$ ,<sup>29</sup> there is a clear shift in spectral weight from the gapped excitation to gapless magnetic fluctuations as these systems become non-superconducting. Therefore, the gapped fluctuations present in Fig. 4 point towards strong evidence that superconductivity and magnetism are directly coupled in these systems. For samples which are not bulk superconductors, the gapped magnetic fluctuations are replaced by gapless paramagnetic fluctuations. Our results demonstrate a direct coupling between superconductivity and antiferromagnetism and, most importantly, the iron doping on the interstitial site. These results also demonstrate a change in the wavevector of fluctuations with doping on the interstitial site. In previous neutron scattering experiments, the gapped excitation has been found to occur at a wavevector of  $\mathbf{Q} = [\frac{1}{2}, \frac{1}{2}]$  within the  $ab$  plane; this ordering corresponds to antiferromagnetic coupling along a diagonal of the Fe square sublattice. However, the magnetic ordering within  $\text{Fe}_{1+x}\text{Te}$  occurs with a  $\mathbf{Q} = [\frac{1}{2}, 0]$ , or antiferromagnetic coupling along one side of the Fe square

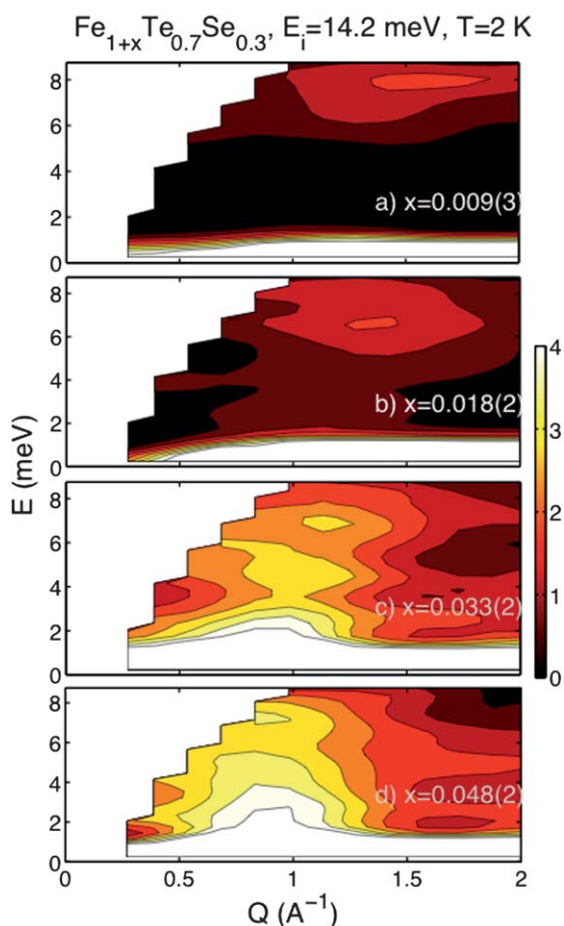


**Fig. 4** Evolution of the excitation spectrum in  $\text{Fe}_{1+x}\text{Te}_{0.7}\text{Se}_{0.3}$  at 2 K, showing the gapped excitation between 6–8 meV for  $x = 0.009(3)$  disappearing to gapless paramagnetic scattering on increase of interstitial iron to  $x = 0.048(2)$ .

sublattice.<sup>11</sup> While the data is powder averaged, the wavevectors are consistent with previous single crystal work, which demonstrates that the magnetic excitations change wavevector from  $[\frac{1}{2} 0]$  to  $[\frac{1}{2} \frac{1}{2}]$  in the presence of superconductivity.<sup>18,19</sup> Indeed, some density functional theory calculations studies have shown that the interstitial iron plays a crucial role on whether  $[\frac{1}{2}, \frac{1}{2}]$ - or  $[\frac{1}{2}, 0]$ -type magnetic interactions will dominate.<sup>30</sup> Thus, our results further advance the theory that magnetic interactions along  $\mathbf{Q} = [\frac{1}{2}, 0]$ , promoted by the interstitial iron sites, are antagonistic to superconductivity in the  $\text{Fe}_{1+x}(\text{Se},\text{Te})$  series.

## Conclusions

We have performed an accurate study of the effects of interstitial iron on the structure and superconductivity of  $\text{Fe}_{1+x}\text{Te}_{1-y}\text{Se}_y$ , and established that superconductivity can occur at different compositions and geometry as long as sufficient interstitial iron, which destroys superconductivity, is removed. This highlights the critical role of the iron concentrations and not Te : Se ratio on the electronic structure. A comparison between the two superconducting compositions of  $\text{Fe}_{1.009(3)}\text{Te}_{0.7}\text{Se}_{0.3}$  and  $\text{Fe}_{1.008(3)}\text{Te}_{0.48(1)}\text{Se}_{0.52(2)}$  revealed some notable differences between their two structure. Nevertheless they show similar superconducting transition temperatures that demonstrates the robustness of

superconductivity in the  $\text{Fe}(\text{Te},\text{Se})$  series. It will be interesting to evaluate the full phase diagram to establish whether  $\text{Fe}_{1+x}\text{Te}$  or composition close to  $\text{Fe}_{1+x}\text{Te}$  can support superconductivity given sufficient removal of interstitial iron.

## Notes and references

- J. Paglione and R. L. Greene, *Nat. Phys.*, 2010, **6**, 645.
- Y. Kamihara, T. Watanabe, M. Hirano and H. Hosono, *J. Am. Chem. Soc.*, 2008, **130**, 3296.
- F. C. Hsu, J. Y. Luo, K. W. Yeh, T. K. Chen, T. W. Huang, P. M. Wu, Y. C. Lee, Y. L. Huang, Y. Y. Chu, D. C. Yan and M. K. Wu, *Proc. Natl. Acad. Sci. U. S. A.*, 2008, **105**, 14262–14264.
- K. W. Yeh, T. W. Huang, Y. L. Huang, T. K. Chen, F. C. Hsu, P. M. Wu, Y. C. Lee, Y. Y. Chu, C. L. Chen, J. Y. Luo, D. C. Yan and M. K. Wu, *Europhys. Lett.*, 2008, **84**, 37002.
- Y. Mizuguchi, F. Tomioka, S. Tsuda, T. Yamaguchi and Y. Takano, *Appl. Phys. Lett.*, 2009, **94**, 012503.
- T. M. McQueen, Q. Huang, V. Ksenofontov, C. Felser, Q. Xu, H. Zandbergen, Y. S. Hor, J. Allred, A. J. Williams, D. Qu, J. Checkelsky, N. P. Ong and R. J. Cava, *Phys. Rev. B: Condens. Matter Mater. Phys.*, 2009, **79**, 014522.
- Y. Mizuguchi, F. Tomioka, S. Tsuda, T. Yamaguchi and Y. Takano, *Appl. Phys. Lett.*, 2008, **93**, 152505.
- S. Medvedev, T. M. McQueen, I. A. Troyan, T. Palasyuk, M. I. Erements, R. J. Cava, S. Naghavi, F. Casper, V. Ksenofontov, G. Wortmann and C. Felser, *Nat. Mater.*, 2009, **8**, 630–633.
- S. Margadonna, Y. Takabayashi, Y. Ohishi, Y. Mizuguchi, Y. Takano, T. Kagayama, T. Nakagawa, M. Takata and K. Prassides, *Phys. Rev. B: Condens. Matter Mater. Phys.*, 2009, **80**.
- M. J. Pitcher, T. Lancaster, J. D. Wright, I. Franke, A. J. Steele, P. J. Baker, F. L. Pratt, W. T. Thomas, D. R. Parker, S. J. Blundell and S. J. Clarke, *J. Am. Chem. Soc.*, 2010, **132**, 10467–10476.
- W. Bao, Y. Qiu, Q. Huang, M. A. Green, P. Zajdel, M. R. Fitzsimmons, M. Zhernenkov, S. Chang, M. H. Fang, B. Qian, E. K. Vehstedt, J. H. Yang, H. M. Pham, L. Spinu and Z. Q. Mao, *Phys. Rev. Lett.*, 2009, **102**, 247001.
- E. E. Rodriguez, P. Zavalij, P. Y. Hsieh and M. A. Green, *J. Am. Chem. Soc.*, 2010, **132**, 10006–10008.
- B. C. Sales, A. S. Sefat, M. A. McGuire, R. Y. Jin, D. Mandrus and Y. Mozharivskiy, *Phys. Rev. B: Condens. Matter Mater. Phys.*, 2009, **79**, 094521.
- P. Zajdel, P.-Y. Hsieh, E. E. Rodriguez, N. P. Butch, J. D. Magil, J. Paglione, P. Zavalij, M. R. Suchomel and M. A. Green, *J. Am. Chem. Soc.*, 2010, **132**, 13000.
- T. J. Liu, X. Ke, B. Qian, J. Hu, D. Fobes, E. K. Vehstedt, H. Pham, J. H. Yang, M. H. Fang, L. Spinu, P. Schiffer, Y. Liu and Z. Q. Mao, *Phys. Rev. B: Condens. Matter Mater. Phys.*, 2009, **80**, 174509.
- R. Vienneis, E. Giannini, D. van der Marel and R. Cerny, *J. Solid State Chem.*, 2010, **183**, 769–775.
- M. Bendele, P. Babkevich, S. Katrych, S. N. Gvasaliya, E. Pomjakushina, K. Conder, B. Roessli, A. T. Boothroyd, R. Khasanov and H. Keller, *Phys. Rev. B: Condens. Matter Mater. Phys.*, 2010, **82**, 212504.
- T. J. Liu, J. Hu, B. Qian, D. Fobes, Z. Q. Mao, W. Bao, M. Reehuis, S. A. J. Kimber, K. Prokes, S. Matas, D. N. Argyriou, A. Hiess, A. Rotaru, H. Pham, L. Spinu, Y. Qiu, V. Thampy, A. T. Savici, J. A. Rodriguez and C. Broholm, *Nature Mater.*, 2010, **31**, 716.
- M. D. Lumsden, A. D. Christianson, E. A. Goremychkin, S. E. Nagler, H. A. Mook, M. B. Stone, D. L. Abernathy, T. Guidi, G. J. MacDougall, C. de la Cruz, A. S. Sefat, M. A. McGuire, B. C. Sales and D. Mandrus, *Nat. Phys.*, 2010, **6**, 182–186.
- J. Rodriguez-Carvajal, *Phys. B*, 1993, **192**, 55.
- S. L. Bud'ko, P. C. Canfield, A. S. Sefat, B. C. Sales, M. A. McGuire and D. Mandrus, *Phys. Rev. B: Condens. Matter Mater. Phys.*, 2009, **80**, 134523.
- A. Martinelli, A. Palenzona, M. Tropeano, C. Ferdeghini, M. Putti, M. R. Cimberle, T. D. Nguyen, M. Affronte and C. Ritter, *Phys. Rev. B: Condens. Matter Mater. Phys.*, 2010, **81**, 094115.

- 23 N. C. Gresty, Y. Takabayashi, A. Y. Ganin, M. T. McDonald, J. B. Claridge, D. Giap, Y. Mizuguchi, Y. Takano, T. Kagayama, Y. Ohishi, M. Takata, M. J. Rosseinsky, S. Margadonna and K. Prassides, *J. Am. Chem. Soc.*, 2009, **131**, 16944–16952.
- 24 H. A. Mook, M. D. Lumsden, A. D. Christianson, S. E. Nagler, B. C. Sales, R. Y. Jin, M. A. McGuire, A. S. Sefat, D. Mandrus, T. Egami and C. dela Cruz, *Phys. Rev. Lett.*, 2010, **104**, 187002.
- 25 Y. M. Qiu, W. Bao, Y. Zhao, C. Broholm, V. Stanev, Z. Tesanovic, Y. C. Gasparovic, S. Chang, J. Hu, B. Qian, M. H. Fang and Z. Q. Mao, *Phys. Rev. Lett.*, 2009, **103**, 067008.
- 26 A. D. Christianson, E. A. Goremychkin, R. Osborn, S. Rosenkranz, M. D. Lumsden, C. D. Malliakas, I. Todorov, H. Claus, D. Y. Chung, M. G. Kanatzidis, R. Bewley and T. Guidi, *Nature*, 2008, **456**, 930.
- 27 C. Stock, C. Broholm, J. Hudis, H. J. Kang and C. Petrovic, *Phys. Rev. Lett.*, 2008, **100**, 087001.
- 28 O. Stockert, J. Arndt, A. Schneidewind, H. Schneider, H. S. Jeevan, C. Geibel, F. Steglich and M. Loewenhaupt, *Phys. B*, 2008, **403**, 973.
- 29 C. Stock, W. J. L. Buyers, R. Liang, D. Peets, Z. Tun, D. Bonn, D. N. Hardy and R. J. Birgeneau, *Phys. Rev. B: Condens. Matter Mater. Phys.*, 2004, **69**, 014502.
- 30 L. Zhang, D. J. Singh and M. H. Du, *Phys. Rev. B: Condens. Matter Mater. Phys.*, 2009, **79**, 012506.